Scattering of GeV electrons and scaling within the mean field theory approach

A. Mariano
Departamento de Física, Facultad de Ciencias Exáctas, Universidad Nacional de La Plata, cc.67, 1900 La Plata, Argentina

Recibido el 7 de enero de 2005; aceptado el 30 de enero de 2005

Electron scattering by nuclei at high momentum transfers is studied within the Fermi smearing approximation (FSA), where binding effects on the struck nucleon are introduced via the relativistic mean field theory (MFT). The model naturally preserves electromagnetic current conservation, since the response tensor for an off-shell nucleon conserves the same form that for a free one but with an effective mass. Different parameterizations for the inelastic nucleon structure function, are used. We also analyze the behavior of the experimental nuclear response in terms of the scaling variable y associated to the model. Recent CEBAF data for the inclusive cross section of 4.05 GeV electrons on ^{56}Fe, are well reproduced for all measured geometries. The theoretical scaling function describes properly the trend of the experimental data, except at high values of Q^2 and large negative values of y. Future improvements to the model are proposed.

Keywords: Inelastic electron scattering; Relativistic scattering; Scaling laws.

La dispersión de electrones a altas transferencias de impulso es estudiada usando la distribución de momentos de un nucleón, mientras que los efectos de ligadura se introducen mediante la teoría de campo medio relativista. El modelo naturalmente conserva la corriente electromagnética, ya que el tensor respuesta para un nucelón fuera de la capa de masas mantiene la mísma forma que la de un nucleón libre pero con una masa efectiva. Diferentes parametrizaciones de la respuesta inelástica del nucleón son usadas. También analizamos la respuesta nuclear experimental en términos de la variable y de escaleamiento asociada al modelo. Los datos recientes del CEBAF para la sección eficaz inclusiva de electrones de 4.05 GeV sobre ^{56}Fe, son bien reproducidos para todas las geometrías medidas. La función de escaleamiento teórica describe propiamente la tendencia de los datos experimentales, excepto a valores altos de Q^2 y valores negativos de y. Se proponen futuras mejoras al modelo.

Descriptores: Dispersion inelastica de electrones; Dispersion relativista; Leyes de escalamiento.

PACS: 25.30.Dh; 11.80-m; 89.75.Da

1. Introduction

Inclusive electron-nucleus scattering experiments performed in different regions of the square four-momentum q^2 ($q \equiv (\omega, \mathbf{q})$) and energy ω transfers, provide information on the nuclei constituents and excited degrees of freedom. The regions are:

(i) the *quasielastic scattering* region, $\omega \leq Q^2/2M$, with M being the nucleon mass and $Q^2 \equiv -q^2 > 0$, where experimental data can be analyzed in terms of scaling variables providing information on nuclear dynamics and the nucleon momentum distribution;

(ii) the *inelastic scattering* region, $\omega \geq Q^2/2M + M_\pi$, with M_π being the pion mass, where nucleon resonances are excited and medium induced modifications of their properties can be studied;

(iii) the *deep inelastic scattering* region,

$$W \equiv \sqrt{(p+q)^2} \geq 2GeV,$$
$$Q^2 \geq 1(GeV/c)^2,$$

being p the initial nucleon four-momentum, where possible modifications of quarks and gluon distributions in the nucleon induced by the medium can be investigated. In the later case the response function also reflects the presence of 6-quark bags in the nuclear wave function.

Electron scattering from nuclei has been analyzed in the past within the domain

$$Q^2 \lesssim 1(GeV/c)^2 (\mathrm{q} \equiv |\mathbf{q}| \lesssim 1\mathrm{GeV/c}) \qquad [1,2].$$

Many observables were properly described by the nonrelativistic nuclear many-body theory with, if necessary, the inclusion of the isobar Δ degree of freedom and meson exchange currents. Examples are the descriptions of the longitudinal and transverse response function; and the evaluation of the Coulomb sum rule [3–5]. Nevertheless, starting from the NE3 SLAC experiment [6] and with the advent of the CEBAF [7] with electron energies of the order of 4 GeV, we are able to reach momentum transfers with $Q^2 > 1$ (GeV/c)^2 ($\mathrm{q} > 1$ GeV/c) and two new features appear now:

i) after the scattering process the struck nucleon is relativistic, having momenta of the order of the nucleon mass;

ii) the probability for exciting internal degrees of freedom of the nucleon (nucleon inelastic response) becomes increasingly important for such momenta transfers.

Another important property to be analyzed is the y scaling, which has been introduced by West [8] and Kamazoe [9], being y the minimum momentum of the struck nucleon along the virtual photon direction. They showed that within the

impulse approximation, and when the quasielastic scattering is the dominant reaction mechanism, a scaling function $F(y, Q^2)$ can be extracted from the measured cross section, which at high Q^2 values scales depending only on y. Finally, at such large Q^2 values, it is also valid to ask about the importance of the final state interaction (FSI) between the emerging nucleon (or hadron) and the residual nucleons , and about the way this interaction influences the cross section and the scaling.

The ideal theoretical starting point should be a relativistically covariant theory of nuclei. However, such an approach is not practicable due to the difficulties in treating meson exchange interactions. In fact in the past, data coming from the NE3 SLAC experiment [6] were analyzed with different variants of the plane wave impulse approximation (PWIA).

One of the first PWIA calculations included one-hole (1h) and two-particle - one-hole (2p-1h) excitations[i] in the residual nucleus, and without including the FSI [10]. In this way the cross sections, when expressed in terms of the well known Bjorken variable $x \equiv Q^2/(2M\omega)$, have been fairly well reproduced in the quasielastic peak[ii] ($x \simeq 1$) and inelastic ($x < 1$) regions, while they were underestimated for $x > 1$. Both, the quasielastic and inelastic cross sections regions are strongly overestimated when the spectral function was approximated by the momentum distribution (FSA).

In order to correct the above mentioned discrepancies at $x > 1$, the FSI is introduced in several different ways. For instance, the discrepancy is circumvented in the region $1 < x < 2$, when the PWIA is extended introducing pair correlations [11]. For $x > 2$ more than two nucleons could be involved in the scattering process and thus the use of an optical potential is required [12]. Benhar *et al.* [13] have improved the PWIA results by introducing the FSI through an optical potential and by generating a folding function from the multiple-scattering Glauber theory. An alternative scheme to the PWIA model has been introduced by Rinat and Taragin [14], being the FSI is introduced through binary collisions between knocked-on nucleon and a nucleon from the nucleus core. Results from CEBAF 4.05 GeV electron scattering [7] on ^{56}Fe are well reproduced for $x < 1$ in this case, and a satisfactory correspondence in the left hand side neighborhood of the quasielastic peak $x \gtrsim 1$ is obtained [15]. Nevertheless, in the low energy lost region the calculated cross section overestimates the data by a factor up to 2-10 for all angles θ, and this discrepancy is associated to uncertainties in the momentum distribution used in the calculation.

As matter of fact, independently of the implemented approach, the scaling function behavior of the model has been analyzed and compared with the data, leading to different versions of the scaling variable. Between them we mention the y scaling variable from Refs. 11 and 13, the y_G Gurvitz's one from Ref. 15, and the y_{WC} used by Ciofi and West in Refs. 16 and 17. All these variables were obtained from the *"same"* energy conservation relation, and the differences between them come from the approximation adopted in each case for the nucleon dynamic (relativistic or not), binding effects and the residual nucleus excitation energy. FSI play an important role in the description of the experimental scaling function. For example, for the naive PWIA the theoretical scaling function is an increasing function of the Q^2 variable, which reach the experimental data only asymptotically at large Q^2 values. This contradicts the trend of the data, which decrease when Q^2 is increased for a fix value of the usual y scaling variable, being this ascribed to the fact that FSI are more important at small Q^2.

In the present work we implement a FSA where the binding effects are introduced through the struck nucleon kinematics which is described within the mean field theory based on quantum hadrodynamics (QHD) [18], and within a nuclear matter framework. This should be a fair approach as the electron probes a region of dimensions $1/\mathrm{q}$, and as at momentum transfers high enough , the surface effects in nuclei are supposed to be of minor importance. The FSI is also included in some extent within the present approach since the nucleon is bounded before and after the interaction with the photon, and therefore acquires an effective mass. The Fermi smearing effects are described here with a momentum distribution generated by a perturbation scheme in a 0p0h + 2p2h + 4p4h configuration space for the initial nucleus. In this way in the residual nucleus we have 1h, 2p3h, 4p5h, 1p2h,and 3p4h excitations when the struck nucleon is removed. We analyze as well, different parameterizations for the inelastic nucleon response measured at SLAC. Finally, we also discuss the scaling behavior of the model, which results in a stringent test of the FSA+MFT approach, based on the evaluation of the theoretical scaling function.

The paper is organized as follows. In Sec. 2 we summarize the FSA+MFT model for the nuclear response and display the corresponding expression for the cross section. In Sec. 3 we describe the used momentum distribution. The scaling variable and the scaling function within the present model are worked out in Sec. 4. Finally, the results are shown in Sec. 5 and the conclusions are drawn in Sec. 6.

2. Cross section and nuclear response model

In the Born approximation the $A(e, e')A'$ differential cross section reads

$$\frac{d^2\sigma}{d\Omega' d\epsilon'} = \frac{e^2}{\mathrm{q}^4}\frac{\mathrm{k}'}{\mathrm{k}} L^{\mu\nu}(k, k') W^A_{\mu\nu}(\omega, \mathbf{q}), \qquad (1)$$

being $\mathrm{k}, \mathrm{k}' \equiv |\mathbf{k}|, |\mathbf{k}'|$, $W^A_{\mu\nu}$ the nuclear response tensor, $L^{\mu\nu}(k, k') = 1/2[k'^\mu k^\nu + k^\mu k'^\nu + (q^2/2 - m^2/2)g^{\mu\nu}]$ the lepton tensor describing incoming and outgoing plane-wave electron states of four-momentum $k = (\epsilon \equiv \sqrt{\mathbf{k}'^2 + m^2}, \mathbf{k})$ and $k' = (\epsilon' \equiv \sqrt{\mathbf{k}'^2 + m^2}, \mathbf{k}')$ respectively, and $\Omega' \equiv (\theta, \phi)$ the scattering angle. The PWIA lies on the following assumptions:

i) the nuclear current operator can be written as the sum of the one-body nucleon currents;

ii) the target decays virtually into a on-shell (A-1) nucleus (spectator) and the off-shell ($p^2 \neq M^2$) struck nucleon, of four-momentum $p = (p_0, \mathbf{p})$; and

iii) the nucleon that absorbs the photon is the same that leaves the target without interaction with the spectator, the final state interactions (FSI) being dropped. Under these assumptions, the nuclear response can be expressed as a convolution [10]

$$W^A_{\mu\nu}(\omega, \mathbf{q}) = \sum_{m_t} \int dE d\mathbf{p} P^{m_t}(E, \mathbf{p}) w^{m_t}_{\mu\nu}(p, q), \qquad (2)$$

of the nucleon response $w^{m_t}_{\mu\nu}(p, q)$ (m_t=p and n for protons and neutrons respectively) with the nuclear spectral function $P^{m_t}(E, \mathbf{p})$. This gives the joint probability of finding a nucleon with three momentum $\mathbf{p}$ inside the target nucleus, and remove it with an energy $E = E_B + E^{\text{exc}}_{A-1}$. $E_B = M_{A-1} + M - M_A$ is the nucleon binding energy and E^{exc}_{A-1} the excitation energy in which the residual nucleus is left. We will work within the FSA $P^{m_t}(E, \mathbf{p}) \sim n^{m_t}(\mathbf{p})\delta(E - E_B)$, giving $n^{m_t}(\mathbf{p})$ the probability of finding a nucleon with momentum $\mathbf{p}$, and isospin m_t in the target $|0_A\rangle$.

Notice that for an off-shell nucleon, the energy p_0=$p_0(E, \mathbf{p})$ depends on its removing energy and its three-momentum, thus to implement the PWIA or any extension including FSI one must address some important questions. First, the nucleon structure function is determined experimentally from proton or deuteron scattering on on-shell (free) targets, being $p^2 = M^2$ (or $p_0 = E_{\mathbf{p}} \equiv \sqrt{\mathbf{p}^2 + M^2}$). In our case we treat with an off-shell bounded nucleon with $p_0 \neq E_{\mathbf{p}}$, and $p_0 = p_0(E, \mathbf{p})$ depends on how the binding effects are included. Second, we need to extend the on-shell nucleon structure function to the off-shell regime to use it as input in the nuclear response calculation. The minimal hypothesis adopted in majority of works is to assume that $w^{m_t(\text{off-shell})}_{\mu\nu}(p, q) = w^{m_t(\text{on-shell})}_{\mu\nu}(\widetilde{p}, \widetilde{q})$, where $\widetilde{p}$ and $\widetilde{q}$ depend on the off-shell prescription adopted for $p_0 = p_0(E, \mathbf{p})$. Third, whatever is the $(\widetilde{p}, \widetilde{q})$ pair we have a lack of the electromagnetic gauge invariance because $w^{m_t(\text{off-shell})}_{\mu\nu} q^\nu \neq 0$, due to the on-shell to off-shell extension. This brings in additional complications, a procedure being required to restore current conservation [10, 19].

In our case the nucleon will be bounded by interaction with the scalar ϕ and vector V_μ mesons fields, within the framework of quantum hadrodynamics(QHDI) [18]. The nucleus response tensor is the Lorentz invariant amplitude and reads [20]

$$\begin{aligned} W^A_{\mu\nu}(\omega, \mathbf{q}) = {} & \frac{\mathrm{k} M_A}{\sqrt{(k.P_A)^2 - m^2 M_A^2}} \frac{V}{(2\pi)^3} \\ & \times \sum_{\mathbf{p}' m'_s m'_t} \sum_f \langle P_A | \hat{J}(0)_\mu | p' m'_s m'_t, P^f_{A-1} \rangle \\ & \times \langle p' m'_s m'_t, P^f_{A-1} | \hat{J}(0)_\nu | P_A \rangle \\ & \times (2\pi)^4 \delta(P_A + k - k' - P^f_{A-1} - p'), \end{aligned} \qquad (3)$$

being $P_A = (M_A, 0)$ and $P^f_{A-1} = (\sqrt{\mathbf{p}_f^2 + (M^f_{A-1})^2}, \mathbf{p}_f)$ the target and residual nucleus four-momentum respectively, with the mass $M^f_{A-1} = M_{A-1} + \omega^f_{A-1}$ including the excitation energy ω^f_{A-1}. The sum on f encloses the set of final residual nucleus states. We also sum on the final states of the struck nucleon with four-momentum $p' = (p'_0, \mathbf{p}')$, spin m'_s and isospin m'_t, with density $V/(2\pi)^3$ in the quantization volume V. $\hat{J}(x) = i\bar{\psi}(x)\Gamma_\mu(q)\psi(x)$ is the effective hadron current density operator with (for the nucleon elastic response case)

$$\Gamma_\mu(q) = F_1(q^2)\gamma_\mu + iF_2(q^2)\frac{\kappa}{2M}\sigma_{\mu\nu}q^\nu,$$

being $\psi(x)$ and κ the nucleon field and anomalous magnetic moment, respectively.

We are going develop on the same footing the nuclear response calculation within the mean field theory (MFT) (where the meson fields are approximated by their vacuum spectation, *i.e.* constant, values), and in the relativistic Hartree approximation RHA [18] (where vacuum fluctuation corrections are added to the MFT results). Later, when we compare the calculated cross section with the data, the RHA election will be justified. The nucleon field is expanded as

$$\begin{aligned} \psi(x) = \frac{1}{\sqrt{V}} \sum_{\mathbf{p} m_s m_t} \sqrt{\frac{M^*}{E^*_{\mathbf{p}}}} \big[& u(\mathbf{p} m_s m_t) a_{\mathbf{p} m_s m_t} e^{ip\cdot x} \\ & + b^\dagger_{\mathbf{p} m_s m_t} v(\mathbf{p} m_s m_t) e^{-ip\cdot x} \big], \end{aligned} \qquad (4)$$

where the spinors $u(\mathbf{p} m_s m_t)$ are solutions of the Dirac equation

$$(\boldsymbol{\alpha}\cdot\mathbf{p} + \beta M^*) u(\mathbf{p} m_s m_t) = (p_0 - C_V^2 \frac{\rho_B}{M^2}) u(\mathbf{p} m_s m_t),$$

and single particle spectrum is given by

$$p_0 = C_V^2 \frac{\rho_B}{M^2} + E^*_{\mathbf{p}},$$

with $E^*_{\mathbf{p}} = \sqrt{\mathbf{p}^2 + M^{*2}}$ and $M^* \equiv M + \Sigma(C_S, M^*)$. $M^* < M$ is the effective mass acquired by the nucleon by action of the attractive scalar field and is determined self-consistently [18] through the scalar self-energy $\Sigma \equiv \Sigma_{MFT}$ or Σ_{RHA}

$$\Sigma_{MFT}(M^*) = -\frac{C_S^2}{M^2}\frac{4}{(2\pi)^3}\int_0^{p_F} d\mathbf{p} \frac{M^*}{\sqrt{\mathbf{p}^2 + M^{*2}}},$$

$$\Sigma_{RHA}(M^*) = \Sigma_{MFT}(M^*) + \Delta M^*,$$

with

$$\Delta M^* = \frac{C_S^2}{M^2}\frac{2}{(2\pi)^2}\left[M^{*3} ln\left(\frac{M^*}{M}\right) M^2(M-M^*) - \frac{5}{2}M(M-M^*)^2 + \frac{11}{6}(M-M^*)^3\right]. \quad (5)$$

Σ_{MFT} includes the tadpole diagram a) in the Fig. 1, retaining in its evaluation only the contribution from nucleons in the filled Fermi sea in the nucleon propagator (tick full lines). Σ_{RHA} includes the same diagram but the full nucleon propagator (which encloses the contribution of the occupied negative-energy states) is used in the evaluation of the self-energy. Then the MFT or the RHA are derived by summing up the self-energy to all orders through the self-consistent determination of M^*, being this procedure convergent in both cases. The first term in $E^*_{\mathbf{p}}$ accounts for the action of the repulsive vector field. C_V and C_S are the two free parameters [21], fixed to reproduce the experimental binding energy per nucleon of -16 MeV at the Fermi momentum $p_F = 1.42 fm^{-1}$ (or the baryon density $\rho_B = 0.19 fm^{-3}$) for the normal nuclear matter, getting

$$C_S^2 \equiv \quad g_S^2\left(\frac{M^2}{m_S^2}\right) = 267.1 \qquad C_V^2 \equiv g_V^2\left(\frac{M^2}{m_V^2}\right) = 195.9,$$

where g_S and g_V, and, m_S and m_V are the coupling constants and masses of the scalar and vector mesons, respectively.

Assuming that the residual nucleus is left in its ground state and adopting the prescriptions ii) and iii) mentioned above, the response tensor can be obtained from Eqs. (3) to (5) as

$$W^A_{\mu\nu}(q) = 2\sum_{m_t}\int d\mathbf{p}\frac{M^*}{E^*_{\mathbf{p}}} n^{m_t}(\mathbf{p}) w^{m_t}_{\mu\nu}(p^*, q), \quad (6)$$

where the factor 2 resembles the sum over spin states, and

$$w^{m_t}_{\mu\nu}(p^*,q) = w^{m_t}_{e1}(Q^2,\nu^*)\left[-g_{\mu\nu} + \frac{q_\mu q_\nu}{q^2}\right] + w^{m_t}_{e2}(Q^2,\nu^*)\left[\frac{p^*_\mu}{M^*} - \nu^*\frac{q_\mu}{q^2}\right]\left[\frac{p^*_\nu}{M^*} - \nu^*\frac{q_\nu}{q^2}\right], \quad (7)$$

with $p^* = (E^*_{\mathbf{p}}, \mathbf{p})$ and[iii] $\nu^* = p^*\cdot q/M^*$. $n^{m_t}(\mathbf{p})$ is the nucleon momentum distribution in the target ground state $|0_A\rangle$.

$$n^{m_t}(\mathbf{p}) = \frac{V}{(2\pi)^3}\langle 0_A|a^\dagger_{\mathbf{p}m_s m_t} a_{\mathbf{p}m_s m_t}|0_A\rangle, \quad (8)$$

normalized as $2\int d\mathbf{p}\; n^{m_t}(\mathbf{p}) = N^{m_t}$, with $N^{m_t} = Z, N$ for $m_t = p, n$. The elastic Lorentz scalar functions present in (7) are

$$w^{m_t}_{e1}(Q^2,\nu^*) = \tau G_M^{m_t 2}\left(Q^2\right)\delta(\nu^* - \frac{Q^2}{2M^*}) \quad (9)$$

$$w^{m_t}_{e2}(Q^2,\nu^*) = \frac{G_E^{m_t 2}(Q^2) + \tau G_M^{m_t 2}(Q^2)}{1+\tau}\delta \times\left(\nu^* - \frac{Q^2}{2M^*}\right) \quad (10)$$

where $G_E^{m_t}(Q^2) = F_1^{m_t}(Q^2) - F_2^{m_t}(Q^2)\kappa^{m_t}\tau$ and $G_M^{m_t}(Q^2) = F_1^{m_t}(Q^2) + F_2^{m_t}(Q^2)\kappa^{m_t}$ are the electric and magnetic form factors, and $\tau = Q^2/4M^{*2}$. In the numerical calculations we adopt the Sachs form for them, assuming that they do not change in the nuclear medium. Equations (7), (9) and (10) show that the MFT or RHA lead to the prescription $w^{m_t\text{(off-shell)}}_{\mu\nu}(p,q) = w^{m_t\text{(on-shell)}}_{\mu\nu}(p^*,q)$ and $w^{\text{(off-shell)}}_{e\ 1,2}(Q^2,\nu) = w^{\text{(on-shell)}}_{e\ 1,2}(Q^2,\nu^*)$, for the elastic case. The nucleon spinors carry a four momentum p^* being $p^{*2} = M^{*2}$, and as $M^* < M$ this makes us remember that the struck nucleon is bounded. Lorentz , parity and gauge invariances are now also fulfilled as were for a nucleon of mass M, as consequence of the form of the Eq. (7).

For $Q^2 > 1$ (GeV/c)^2 the probability of exciting internal states of the nucleon is important, and a replacement

$$w^{m_t}_{e\ 1,2} \to w^{m_t}_{1,2} = w^{m_t}_{e1,2} + w^{m_t}_{i1,2},$$

in (7) should be done, adding an inelastic contribution $w^{m_t}_{i1,2}$. For $w^{m_t}_{i1,2}$ we use different parametric fits done at SLAC for $p(e,e')p'$ and $d(e,e')d'$ data through the Eqs. (7), with M^*=M. We assume that the recipe $w^{off-shell}_{i1,2}(Q^2,\nu) = w^{on-shell}_{i1,2}(Q^2,\nu^*)$, which naturally appears in the elastic case, is also valid for the inelastic nucleon response function. Finally, the decomposition $w^{m_t}_{1,2} = w^{m_t}_{e1,2} + w^{m_t}_{i1,2}$ leads also to split the inclusive cross Sec. (1) in elastic and inelastic contributions.

3. Nucleon momentum distribution

The momentum distribution $n^{m_t}(\mathbf{p})$ is calculated in a 0p0h + 2p2h + 4p4h configuration space for the A-target, being

$$|0_A\rangle = \mathcal{N}\left[|0p0h\rangle + \sum_{p's,h's} c_{p_1p_2h_1h_2}|p_1p_2h_1h_2\rangle + \sum_{p's,h's} c_{p_1p_2p_3p_4h_1h_2h_3h_4}|p_1p_2p_3p_4h_1h_2h_3h_4\rangle\right], \quad (11)$$

where these $|npnh\rangle$, (with $n = 0, 2, 4$) stand for the unperturbed states. In this way in the residual nucleus we have 1h, 2p3h, 4p5h, 1p2h,and 3p4h excitations when the struck nucleon is removed. The residual nucleon-nucleon interaction is included within a perturbative approach as in Ref. 22 by expanding the coefficients c_{2p2h} and c_{4p4h} up to the first and second order, respectively being

$$c_{p_1p_2h_1h_2} = -\frac{\langle p_1p_2h_1h_2|\hat{V}|0p0h\rangle}{(2!)^2 E_{p_1p_2h_1h_2}},$$

$$c_{p_1p_2p_3p_4h_1h_2h_3h_4} = \frac{\langle 0p0h|\hat{V}|p_1p_2h_1h_2\rangle\langle p_1p_2h_1h_2|\hat{V}|p_1p_2p_3p_4h_1h_2h_3h_4\rangle}{(4!)^2 E_{p_1p_2h_1h_2} E_{p_1p_2p_3p_4h_1h_2h_3h_4}}. \quad (12)$$

This "minimum" perturbative scheme allows to include norm corrections $\mathcal{N} = \langle 0_A|0_A\rangle^{-1}$, avoiding in this way contributions of unbalanced disconnected diagrams. Here $\hat{V}$ is the residual interaction, for which a Landau-Migdal parameterization, supplemented by the static one pion exchange potential, this reading

$$\hat{V}(\mathrm{q}) = \sum_I V^I(\mathrm{q}) \mathbf{O}_1^I(\hat{\mathbf{q}}) \cdot \mathbf{O}_2^I(-\hat{\mathbf{q}}) \quad (13)$$

where the quantum numbers $I = T, S, J$ stand, respectively, for the isospin , the spin and the total angular momentum. The operators $\mathbf{O}^I(\hat{\mathbf{q}})$ are defined as

$$\mathbf{O}^{000}(\hat{\mathbf{q}}) = 1; \qquad \mathbf{O}^{010}(\hat{\mathbf{q}}) = i(\hat{\mathbf{q}} \cdot \sigma);$$
$$\mathbf{O}^{011}(\hat{\mathbf{q}}) = (\hat{\mathbf{q}} \times \sigma), \qquad \mathbf{O}^{100}(\hat{\mathbf{q}}) = \tau;$$
$$\mathbf{O}^{110}(\hat{\mathbf{q}}) = i(\hat{\mathbf{q}} \cdot \sigma)\tau \qquad \mathbf{O}^{111}(\hat{\mathbf{q}}) = (\hat{\mathbf{q}} \times \sigma)\tau,$$

and the strengths $V^I(\mathrm{q})$ are defined in Ref. 22 and depend on the usual Landau-Midgal parameters f, f', g and g'. Finally, from Eqs.(11) ,(12) and (13) in a nuclear matter framework, we get

$$n^{m_t}(\mathbf{p}) = \frac{3N^{m_t}}{4\pi \mathrm{p}_F^3}\left[\theta(1-\mathrm{p}) + \delta n^{(2)}(\mathrm{p}) + \delta n^{(4C)}(\mathrm{p})\right], \quad (14)$$

where $\mathrm{p} \equiv |\mathbf{p}|$ is measured in units of the Fermi momentum p_F. The first term is the usual 0p0h Fermi step function, while $\delta n^{(2)}(\mathrm{p})$ and $\delta n^{(4C)}(\mathrm{p})$ (where the superscript C indicates "connected" 4p4h diagrams) enclose 2p2h and 4p4h contributions respectively, which deplete it. The expressions for $\delta n^{(2)}(\mathrm{p})$ and $\delta n^{(4C)}(\mathrm{p})$, are given in Ref. 22.

4. Scaling

It is possible to express the nuclear cross Sec. (6) as the convolution

$$\frac{d^2\sigma}{d\Omega' d\epsilon'} = 2\pi \int_{\mathrm{p}_{min}}^{\mathrm{p}_{max}} d\mathrm{p}\mathrm{p} \sum_{m_t=p,n} n^{m_t}(\mathbf{p}) \frac{d\sigma^{m_t}(\mathrm{p},\omega,\mathbf{q})}{d\Omega'} \times \frac{E^*_{\mathbf{p}} + \omega}{\mathrm{q}}, \quad (15)$$

with the polar averaged single nucleon cross section ($\nu \equiv p.q/M^*$ and $\mathrm{p} \equiv |\mathbf{p}|$)

$$\frac{d\sigma^{m_t}(\mathrm{p},\omega,\mathbf{q})}{d\Omega'} = \frac{d\sigma_M}{d\Omega'} \frac{1}{2\pi} \int dcos\theta_{\mathbf{p}} \int d\phi_{\mathbf{p}} \frac{2M^*}{E^*_{\mathbf{p}}} \frac{\mathrm{pq}}{E^*_{\mathbf{p}} + \omega} \left\{ \left(1 + \frac{p_z}{M^*}\frac{Q^2}{\mathrm{q}\nu}\right)\left(\frac{\nu}{\omega}\right)^2 w_2^{m_t}(Q^2,\nu) - \frac{Q^2}{\mathrm{q}^2} w_1^{m_t}(Q^2,\nu) + \left(\frac{1}{2}\frac{Q^2}{\mathrm{q}^2} + tan^2\frac{\theta}{2}\right)\left[w_1^{m_t}(Q^2,\nu) + w_2^{m_t}(Q^2,\nu)\left(\frac{p_x}{M^*}\right)^2\right]\right\}, \quad (16)$$

where $d\sigma_M/d\Omega'$ is the Mott cross section. The scaling function is defined as

$$F(\omega,\mathbf{q}) = \frac{\frac{d^2\sigma}{d\Omega' d\epsilon'}(\omega,\ \mathbf{q})}{N\ \frac{d\sigma_e^n(\mathrm{p}_{min},\ \omega,\ \mathbf{q})}{d\Omega'} + Z\ \frac{d\sigma_e^p(\mathrm{p}_{min},\ \omega,\ \mathbf{q})}{d\Omega'}} \times \frac{\mathrm{q}}{E_{\mathbf{p}_{min}} + \omega}, \quad (17)$$

where p_{min} corresponds to $\mathbf{p} = \pm \mathrm{p}_{min}\hat{\mathbf{q}}$ and can be obtained from the energy conservation relation $\omega = E^*_{\mathbf{p}+\mathbf{q}} - E^*_{\mathbf{p}}$ as

$$\omega = \sqrt{(\mathrm{q} \pm \mathrm{p}_{min})^2 + M^{*2}} - \sqrt{(\mathrm{p}_{min})^2 + M^{*2}}, \quad (18)$$

which gives

$$\mathrm{p}_{min} = \left| -\frac{\mathrm{q}}{2} + \frac{\omega}{2}\sqrt{\frac{4M^{*2}}{Q^2} + 1} \right|.$$

We also stress here that, because the nucleon momentum distribution $n^{m_t}(\mathbf{p})$ is a rapidly decreasing function of p, we make $\mathrm{p}_{max} \to \infty$ in Eq. (15). The MFT or RHA scaling variable is defined as [23]

$$y = -\frac{\mathrm{q}}{2} + \frac{\omega}{2}\sqrt{\frac{4M^{*2}}{Q^2} + 1}, \quad (19)$$

being $p_{min} = |y|$ for a fixed $(\omega, \mathbf{q})$ pair. At high Q^2 values is $\mathrm{q} \simeq \omega_{qe}$ and $y \simeq (\omega - \omega_{qe})/2$, in such way that $y < 0$

($y > 0$) corresponds to $\omega < \omega_{qe}$ ($\omega > \omega_{qe}$). In this limit and for $y < 0$,

$$\frac{d\sigma^{m_t}}{d\Omega'}\frac{E^*_{\mathbf{p}} + \omega}{\mathrm{q}}$$

in Eq. (15) depends only very weakly on p [10] and therefore it can be factorized out and evaluated at $\mathrm{p} = \mathrm{p}_{\min}$. Additionally, if the contribution of inelastic channels is negligible

$$\left(\frac{d\sigma^{m_t}}{d\Omega'} \simeq \frac{d\sigma^{m_t}_e}{d\Omega'}\right),$$

which should happen at $\omega < \omega_{qe}$, from (15) and (17) we get

$$F(\omega,\ \mathbf{q}) \quad = \quad F(y) \simeq 2\pi \int\limits_{|y|}^{\infty} d\mathrm{p}\mathrm{p}n(\mathrm{p}). \qquad (20)$$

This indicates that, for $Q^2 \to \infty$, F scales in y *i.e.*, it depends only on y and not on (ω, q) or (ω, θ) separately. This peculiar feature can be tested by calculating $F(y, Q^2)$ from (17) and varying Q^2 for a fixed $y < 0$, looking for the approximately constant value given in the Eq. (20).

5. Results

We now compare the differential cross section calculated within our model, with the CEBAF experimental results for ^{56}Fe [7] for the various accessible geometries θ=15, 23, 30, 37, 45, 55, 74°. One of the parameterizations for $w^{m_t}_{i1,2}$ was found by Bodek *et al.* [24] in the kinematical range $1 < Q^2 < 20$ (GeV/c)^2 and $0.1 \leq x \leq 0.77$. The other one was reported by Whitlow [25], and corresponds to the range $0.6 < Q^2 < 30$ (GeV/c)^2 and $0.06 \leq x \leq 0.9$. The functions obtained in these parameterizations are described in detail in Ref. 26, and as they do not cover all the low energy and momentum transfer region of CEBAF, an extrapolation is necessary. Also in this section we compare the dependence of the experimental (F_{exp}) and FSA + RHA theoretical (F_{th}) scaling functions versus y and Q^2 variables. The experimental function F_{exp} is obtained from Eq. (17) using the cross sections reported in the CEBAF 4.05 GeV data for ^{56}Fe [7], divided by the nucleon off-shell elastic cross section, calculated with $w^{m_t}_{1,2} = w^{m_t}_{e1,2}$. The theoretical function F_{th} is also obtained from Eq. (17), being

$$\frac{d^2\sigma}{d\Omega' d\epsilon'}$$

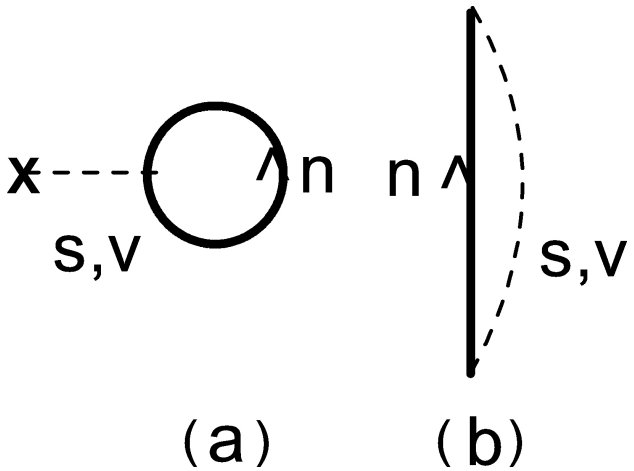

FIGURE 1. (a) Tadpole diagram included in the MFT and RHA self-energies. (b) Tadpole exchange diagram that is added in order to get the relativistic Hartree Fock self-energy. The dashed lines indicate the propagator of the scalar (S) or vector meson (V) that interacts with a nucleon n (full lines).

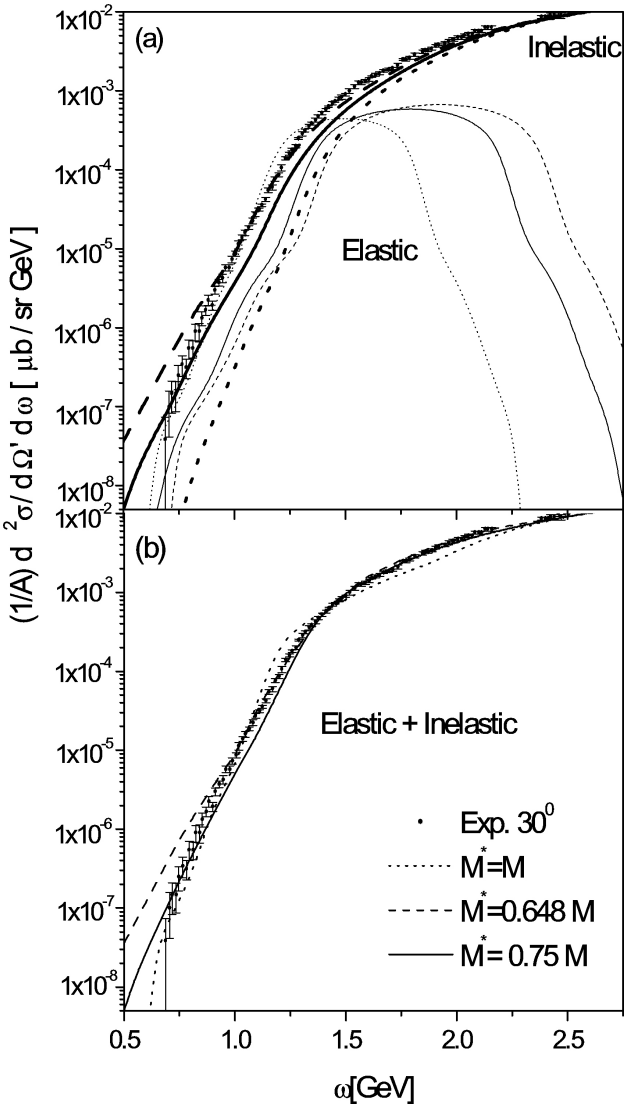

FIGURE 2. We show the sensibility with the effective mass M^* of the quasielastic and inelastic contributions to the cross sections per nucleon for ^{56}Fe. Here the replacement $\epsilon' = \epsilon + \omega$ is done. In the panel (a) both cross sections are shown separately for the values $M^* = 1$, 0.64, and 0.74. Thin lines indicate elastic cross sections while thick lines indicate the inelastic one. In panel (b) the total elastic + inelastic cross section is shown for the different values of M^*. Again, experimental results come from Ref. 7.

evaluated including both elastic and inelastic parts, *i.e.*, with $w^{m_t}_{1,2} = w^{m_t}_{e1,2} + w^{m_t}_{i1,2}$.

Within the MFT and for ^{56}Fe ($p_F = 1.36$ fm^{-1}), $M^* = 0.648M$. This value is too low to reproduce satisfactorily the total cross section since the quasielastic peak is shifted too much to the right and its width ($\Delta\omega_{qe}$) is enlarged in excess, as shown in the Fig. 2. We try to improve the MFT description by adding the vacuum fluctuation corrections to Σ_{MFT}, and go to the RHA where $M^* = 0.74M$. As can be seen in Fig. 2 the RHA the binding-energy shift is more moderated and the width is diminished, getting a better description for the total cross section. This improvement is not casual since as it is well known the RHA yields to the "best" single-particle spectrum in the sense that it minimizes the energy of the whole system. FSI are taken into account in our model at the RHA level. Binding effects are present in the final state, since the nucleon still has mass M^* after absorbing the photon. This simple form of introducing FSI has never been used previously to describe a multi-GeV electron experiment with the inclusion of the inelastic nucleon response, being only described in the past the quasielastic cross section at intermediate energies in the MFT framework [23].

Our results for the total cross section are shown in Fig. 3. As can be seen in, the overall agreement is good for all angles θ, considering that the cross section varies over several orders of magnitude. At $\omega < \omega_{qe}$ ($x > 1$) Withlow's fit seems to be preferred to Bodek's, which is due possibly to differences in the extrapolation for the $x > 1$ range. For $\omega > \omega_{qe}$ ($x < 1$) the behavior is opposite. We see that the model tends to overestimate the $x > 1$ data, in the last two θ values. The inelastic response dominates the cross section at these geometries since $Q^2 \gtrsim 4(GeV/c)^2$, and this overestimation could be also

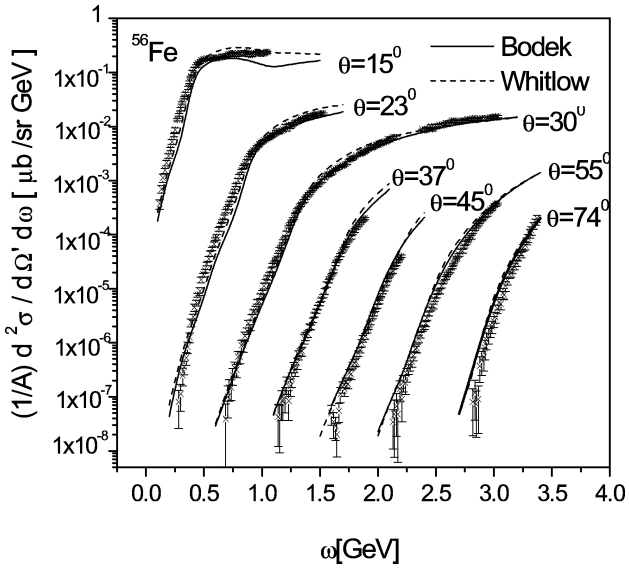

FIGURE 3. Calculated differential cross section per nucleon for different θ geometries for ^{56}Fe. Experimental data come from Ref. 7. Results are shown for both, the fitting of Bodek and Withlow of the inelastic nucleon response, and for a value $M^* = 0.74$ corresponding to the RHA.

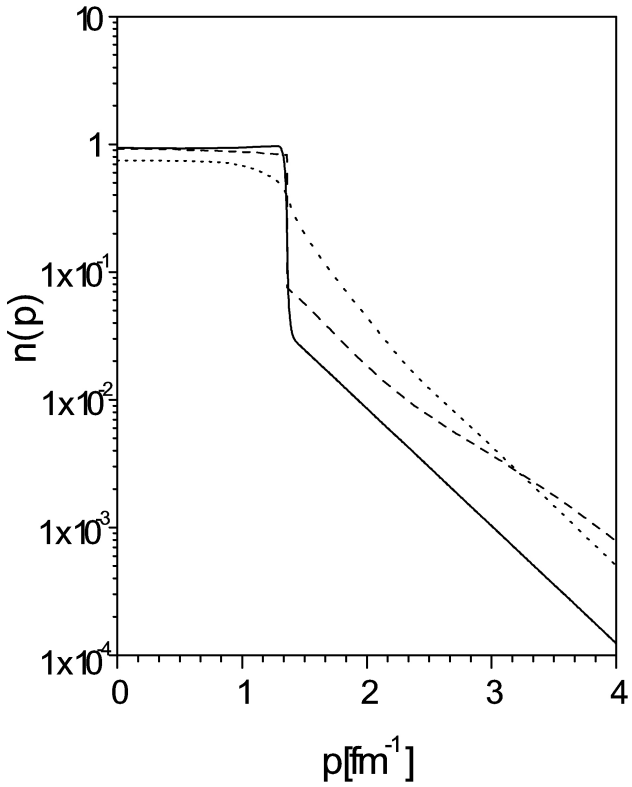

FIGURE 4. Comparison of the nuclear matter momentum distribution used in our calculations (full lines), with its second order approach (dotted lines) and the momentum distribution of Ref. 27 (dashed lines).

as consequence of uncertainties in the extrapolation for $x > 1$. Finally in Figure 4 we show the momentum distribution obtained from the Eq.(14) together with its second order approach, being $\delta n^{(4C)}(\mathrm{p})$ dropped. In the same figure we show the momentum distribution of Ref. 27 (parameterized in [12]), which was obtained within a second order perturbation approach over a set of unperturbed variational wave functions. It is clear that in a second-order approach the momentum distribution is strongly overestimated.

The tendency towards y-scaling is evidenced more clearly when $F(y, Q^2)$ is plotted as a function of Q^2 for y fixed. Experimental and theoretical results for $y = 0$, -0.1, -0.2, -0.3, -0.4 and -0.45 GeV/c, values for which Q^2 falls into the range of the data for each angle, are exhibit in Figure 5. There we see that F_{exp} scales at high Q^2 and tend asymptotically to a constant value for $y \lesssim -0.3$ GeV/c. From the experimental point of view, the overall trend of F_{exp} is satisfactory described within the FSA + RHA, in sense that our model gives an increasing scaling function in terms of Q^2 when is plotted for a fix value of the y, following the experimental data behavior. In contrast to the previous PWIA calculations [10] the scaling function is well reproduced at low Q^2 for small negative y values, which indicates that both the binding effects and FSI are properly accounted for the RHA in this Q^2 range. For $Q^2 \gtrsim 2$ (GeV/c)^2 the inelastic nucleon contribution to the cross section becomes important and dominant. In fact, when the inelastic contribution is

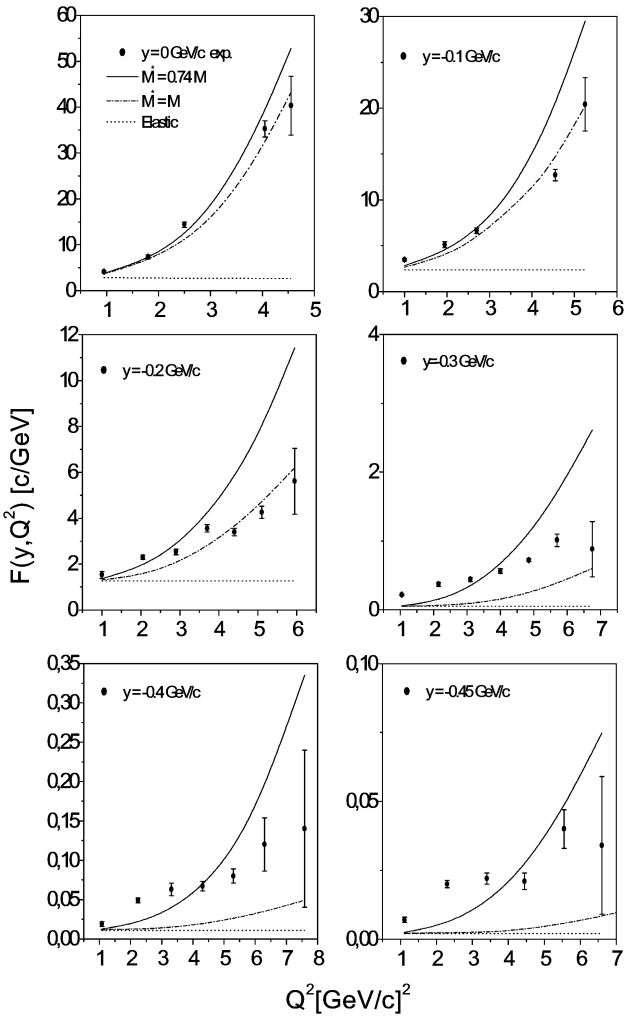

FIGURE 5. Scaling function $F(y, Q^2)$ for ^{56}Fe as a function of Q^2 for different values of the y scaling variable. Theoretical results obtained within our model are shown for the next cases: i) dropping the inelastic structure function (dotted line); ii) including the inelastic structure function by means of the Bodek's fit and using the RHA value $M^* = 0.74M$ (solid line) and the bare mass value (dot-dashed line).

dropped ($w^{m_t}_{1,2} \cong w^{m_t}_{e1,2}$), F_{th} trivially scales to a constant value, which is different to the experimental limit as consequence of dropping $w^{m_t}_{i1,2}$. As can be seen from Fig. 5, the theoretical scaling function F_{th} calculated within the FSA+RHA improves the overall description of the data as y decreases, but underestimate the data at low Q^2 values and overestimates them at high Q^2 domain. This could be ascribed to the way we extrapolate $w^{m_t}_{i1,2}(Q^2, \nu)$ off-shell, which is achieved by making the replacement $M \to M^*$ in ν, being the sensibility to this change also shown in Fig. 5. In fact, when $M^* = M$, which in our approach means to drop binding effects and FSI, F_{th} falls under F_{exp}, specially for large negative y values, evidencing that these effects are important to get the right F_{exp} behavior and its asymptotic limit [7]. One then could conclude that at low Q^2 one should to adopt $M^* < M$, but that for high Q^2values M^* must be increased. In other words, the scaling analysis clearly indicates that a q-dependence on the effective mass M^* is required in order to improve the agreement between data and theoretical results, as it was previously reported in Ref. 19 for $Q^2 \leq 1.3$ (GeV/c)^2, in the context of a different model. To get a more realistic behaviour of the effective mass with q, we must to include the exchange contribution (see Fig. 1(b)) in the self-energy and go to the relativistic Hartree-Fock approximation [28]. The price to be paid is that now we must couple the photon to the intermediate nucleon in diagram (b) from Fig. 1, and calculate the corresponding vertex correction to get gauge invariance.

6. Conclusions

In summary, to treat the scattering of GeV electrons by nuclei we have implemented a new Fermi smearing approach. Binding effects and FSI are introduced through the nucleon effective mass within the RHA, that leads to better results than the plain MFT [26]. In the model, current conservation is preserved naturally without ad-hoc modifications in the structure functions. Fermi smearing effects are introduced through a new momentum distribution that accounts for 2p2h and 4p4h correlations in the target, generated via a perturbative approach in nuclear matter. We get a reasonable overall description of the behavior of the measured cross section at CEBAF, for the scattering of 4.05 GeV electrons on ^{56}Fe. The agreement for all the accessible geometries, has been significantly improved in comparison with previous theoretical studies [15].

Comparison between experimental and theoretical results shows that the theoretical scaling function obtained within our approach describes properly the trend of the experimental recent CEBAF data on inclusive scattering of 4.05 GeV electrons on ^{56}Fe, except at high values of Q^2 and large negative values of y. As a conclusion, it is suggested that a modification of the RHA model capable of producing a q-dependence of the effective nucleon mass M^* is required in order to improve the agreement between the theoretical and experimental results.

Acknowledgements

The work of A. Mariano was supported by Conicet (Argentina).

i. These configurations are originated by picking-up a nucleon from the 0p0h and 2p2h ground state components, respectively.

ii. The quasielastic peak energy for a nucleon at rest corresponds to $\omega_{qe} \equiv Q^2/2M$, which for $\mathrm{q}/M \gg 1$ leads to $\omega_{qe} \simeq \mathrm{q}$.

iii. Q^2 and $\nu = p.q/M$ are commonly used as independent variables for $w_{1,2}^{m_t}$ in the nucleon response.

1. D.B. Day *et al.*, *Phys. Rev. Lett.* **43** (1979) 1143.
2. Z.-E. Meziani, *Nucl. Phys. B* **446** (1985) 113.
3. J.W. Van Order and T.W. Donelly, *Ann. Phys. (N.Y)* **131** (1981) 451.
4. W.M. Alberico, M. Ericson and A. Molinari, *Ann. Phys. (N.Y)* **154** (1984) 356.
5. A. Mariano, E. Bauer, F. Krmpotic, and A.F.R. de Toledo Piza, *Phys. Lett. B* **268** 332 (1991).
6. D.B. Day *et al.*, *Phys. Rev. Lett.* **59** 427 (1987); D.B. Day *et al.*, *Phys. Rev. C* **40** 1011 (1989); D.B. Day *et al.*, *Phys. Rev. C* **48** 1849 (1993).
7. J.R. Arrington *et al.*, *Phys. Rev. Lett.* **82** 2056 (1999).
8. G.B. West , *Phys. Rep.* **18** 263 (1975).
9. Y. Kamazoe, G. Takeda, and H. Matsuzaki, *Prog. Theor. Phys.* **54** 1394 (1975).
10. C. Ciofi degli Atti and S. Simula, *Phys. Rev. C* **43** (1991) 1155; C. Ciofi degli Atti, D.B. Day, and S. Liuti, *Phys. Rev. C* **46** (1991) 1045.
11. C. Ciofi degli Atti and S. Simula, *Phys. Lett. B* **325** (1994) 276.
12. C. Ciofi degli Atti and S. Simula, *Phys. Rev. C* **53** (1996) 1689.
13. O. Benhar *et al.*, *Phys. Rev. C* **44** (1991) 2328.
14. A.S. Rinat and M.F. Taragin, *Nuc. Phys. A* **620** (1997) 417.
15. A.S. Rinat and M.F. Taragin, *Phys. Rev. C* **60** (1999) 044601.
16. C. Ciofi degli Atti and G.B. West, *Phys. Lett. B* **458** (1999) 447.
17. D. Faralli, C. Ciofi degli Atti and G.B. West, nucl-th/9910065 (1999).
18. B.D. Serot and J.D. Walecka, *Adv. Nucl. Phys.* **16** (1986) 1.
19. M.R. Frank, *Phys. Rev. C* **49** (1994) 555; Hungchong Kim, C.J. Horowitz, and M.R. Frank, *Phys. Rev. C* **51** (1994) 792.
20. J.D. Bjorken and S.D. Drell, *Relativistic quantum mechanics* (McGraw-Hill, New York, 1964).
21. J.D. Walecka, *Theoretical Nuclear and Subnuclear Physics* (Oxford University Press, New York, 1995).
22. A. Mariano, F. Krmpotic, and AFR. de Toledo Piza, *Phys. Rev. C***53** (1996) 1664.
23. R. Rosenfelder, *Ann. Phys. (N.Y.)* **128** (1980) 188.
24. A. Bodek and J.L. Ritchie, *Phys. Rev. D* **23** (1981) 1070.
25. L.W. Whitlow, *Ph.D. thesis* SLAC Report No. 357 (1990).
26. T.C. Ferrée and D.S. Koltun, *Phys. Rev. C* **55** (1997) 253
27. S. Fantoni and V.R. Pandharipande, *Nuc. Phys. A* **427**(1984) 473.
28. C.J. Horowitz and B.D. Serot, *Nucl. Phys. A* **399** (1983) 529.